

## MIT Open Access Articles

*Resist roughness Bi-modality as revealed  
by two-dimensional FFT 2D analysis*

The MIT Faculty has made this article openly available. **Please share**  
how this access benefits you. Your story matters.

**Citation:** Gotkis, Yehiel et al. "Resist roughness bi-modality as revealed by two-dimensional FFT 2D analysis." Advances in Resist Materials and Processing Technology XXVI. Ed. Clifford L. Henderson. San Jose, CA, USA: SPIE, 2009. 727345-10. © 2009 SPIE--The International Society for Optical Engineering

**As Published:** <http://dx.doi.org/10.1117/12.813842>

**Publisher:** The International Society for Optical Engineering

**Persistent URL:** <http://hdl.handle.net/1721.1/52649>

**Version:** Final published version: final published article, as it appeared in a journal, conference proceedings, or other formally published context

**Terms of Use:** Article is made available in accordance with the publisher's policy and may be subject to US copyright law. Please refer to the publisher's site for terms of use.



## Resist Roughness Bi-modality as Revealed by Two-dimensional FFT 2D Analysis

Yehiel Gotkis, Leonid Baranov, KLA-Tencor Corporation  
Theodore H. Fedynyshyn, Susan Cann, MIT Lincoln Laboratory

### Abstract

LER/LWR performance is currently considered as one of the major stumbling blocks complicating progress in the semiconductor technology. Line edge scans show that low frequency components clearly dominate the LER Power Spectral Density (PSD), thus implying a large characteristic length (>100-500 nm) phenomenon as the major LER source.

Most of the theoretical analyses aimed to identify the origin of the LER were focused on the combined effect of exposure and CAR action statistics, and failed to explain the origin of this limit, which resulted in suggestions that there is more than just one phenomenon involved in LER generation.

Depth profiling experiments were performed for a broad set of Polymer-PAG-Base combinations. Depth profiling PSD spectra have demonstrated that higher RMS values and correspondingly higher PSD amplitudes are associated with tighter PSD spectrum shifted towards lower frequencies (larger sizes of roughness features), which is very typical for all the cases investigated. The set of the PSD spectra obtained exhibit a pronounced bi-modal structure, indicating that there are at least two clearly noticeable independent roughness-controlling mechanisms.

**Key words:** resists, LER, FFT 2D, PSD analysis, roughness bi-modality.

### INTRODUCTION

LER/LWR performance is currently considered as one of the major stumbling blocks complicating progress in the semiconductor technology. Line edge scans show low frequency components clearly dominating the LER Power Spectral Density (PSD) spectrum, thus implying a large characteristic length (>100-500 nm) phenomenon as the major LER source. Numerous LER improvement efforts (See [1] and references therein) have demonstrated LER to level off asymptotically at  $3\sigma = 4-5$  nm, with practically no further response to resist improvement activity, which gave rise to the term "LER fundamental limit".

Most of the theoretical analyses aimed to identify the origin of the LER were focused on the combined effect of exposure and catalytic CAR action statistics [2-5], and did not explain (and even did not address) the origin of this limit, which resulted in suggestions that there is more than just one CAR phenomenon involved in LER generation [6]. To resolve the LER issue the origin of the long-range ( $10^2$ - $10^3$  nm) LER features must be understood.

Material structures of  $10^2$ - $10^3$  nm scale are known as mesoscopic structures and are subjects of mesoscopic physics - a sub-discipline of condensed-matter physics that focuses on the properties of solids in a size range intermediate between bulk matter and individual atoms or molecules. This structural network modulates interfacial physical and chemical responses, especially catalytic chemistries (like CAR catalytic transformations), which are known to be especially sensitive even to finest material structure/composition variations. Thereby, if the resist film itself or/and resist/processing system interface are meso-structured, it will inevitably affect the roughness response at all the resist processing steps and, as a result, have a significant impact upon the overall surface (and line edge) roughness.

We have employed a technique called resist deconstruction to probe which material factors can also impact resist roughness [7]. This method involves performing a contrast curve and measuring the resulting film roughness with differing degrees of film loss. This technique allowed for the identification of the PAG as a major contributor to IMR [8,9]. Further work identified the inhibition properties of the PAG coupled with PAG segregation during post exposure bake step as significant contributors of IMR and by inference of LWR [10]. A correlation between atomic force microscope (AFM) and chemical force microscope (CFM) responses provided direct evidence that PAG segregation occurred and that this segregation was responsible for the observed film surface roughness [11].

## EXPERIMENTAL

The approach used to probe the structural content at different resist film depths as function of process state and conditions could be formulated as resist roughness depth profiling (RR DP). Silicon wafers with blanket (unpatterned) resist films were immersed into resist developer to allow the film to be dissolved down to different depths. Two versions of this approach were utilized, namely, (a) the exposure dose was varied and the develop time kept constant, and (b) the exposure dose was kept constant and the develop time varied. The residual film surface profile was scanned by AFM. Resist films at different stages of the lithography sequence or at different processing conditions were studied. More details about the RR DP technique were published earlier [7-11].

To probe the resist film structural content at different depths as function of process state and conditions a two dimensional Fourier transform (FFT 2D) and power spectral density (PSD) analysis for the AFM scanned surface profile was performed. In the early stages of this study it was realized that AFM scans could be distorted due to various deficiencies of the AFM scanning procedure (scan baseline distortion). A special routine aimed to deal with the baseline distortions was introduced in the software code.

**Resists.** Depth profiling experiments were performed for a broad set of Polymer-PAG-Base combinations. The 65:20:15 poly(hydroxystyrene-co-styrene-co-t-butylacrylate) (Poly-J) and 66:20:10:4 poly(hydroxystyrene-co-styrene-co-t-butylacrylate-co-methacrylic acid) (Poly-K1) polymers were obtained from DuPont Electronic Polymers. Di(t-butylphenyl)iodonium nonafluoro-1-butanesulfonate (DTBPI-PFBS), di(t-butylphenyl)iodonium perfluorobenzenesulfonate (DTBPI-PFBzS), tri(t-butylphenyl)sulfonium perfluorobenzenesulfonate (TTBPS-PFBzS), tri(phenyl)sulfonium nonafluoro-1-butanesulfonate (TPS-PFBS), and N-hydroxynaphthaldicarboximide perfluorobenzenesulfonate (NHNCI-PFBzS) were obtained from Toyo Gosei Kogyo. Tetrabutyl ammonium hydroxide (TBAH) was obtained from Aldrich Chemical.

Triphenylsulfonium salt 4-(vinyl)benzenesulfonate (VBS-TPS) was prepared by the method of Gonsalves by reacting sodium 4-styrenesulfonate and triphenylsulfonium chloride [8]. Triphenylsulfonium salt 4-(methacryloxy)benzenesulfonate (MBS-TPS) was likewise prepared by the method of Gonsalves by reacting sodium 4-phenosulfonate and methacrylic acid [9]. The TPS-VBS and TPS-MBS based polymers were prepared by free radical polymerization by methods described by in these proceedings [10]. The number after the polymer name refers to the weight percent of PAG monomer in the final polymer.

All monomeric PAG containing resists were formulated based on materials weight percent with 95% polymer, 5% PAG and 0.38% base additive in ethyl lactate solvent except for LUVR-99201 and LUVR-99205 which did not contain a base additive. Table 1 lists material compositions for monomeric PAG containing resists.

**Table 1. Material components of monomeric PAG resists.**

Resist Name	Polymer	PAG	Base
LUVR-99201	Poly-J	DTBPI-PFBS	none
LUVR-99203	Poly-J	DTBPI-PFBS	TBAH
LUVR-99205	Poly-K	DTBPI-PFBS	none
LUVR-99258	Poly-J	TPS-PFBS	TBAH
LUVR-99291	Poly-J	DTBPI-PFBzS	TBAH
LUVR-99292	Poly-J	TTBPS-PFBzS	TBAH
LUVR-99293	Poly-J	NHNCI-PFBzS	TBAH

All polymeric PAG resists were formulated based on materials weight percent with 95% polymer, 5% PAG and 0.38% TBAH in DMSO solvent. The polymeric PAG containing resists were formulated by adjusting the polymer and polymeric PAG content to have the weight percent of the PAG component in the resist equal to that of monomeric PAG resists. Table 2 lists material compositions for polymeric PAG containing resists.

**Table 2. Material components of polymeric PAG resists.**

Resist Name	Polymer	PAG	PAG (%)	Base
LUVR-99395	Poly-J	TPS-VBS	5.0	TBAH
LUVR-99396	Poly-J	P(TPS-VBS-32)	16.6	TBAH
LUVR-99397	Poly-J	P(TPS-VBS-54)	9.2	TBAH
LUVR-99398	Poly-J	TPS-MBS	5.0	TBAH
LUVR-99399	Poly-J	P(TPS-MBS-36)	15.0	TBAH
LUVR-99400	Poly-J	P(TPS-MBS-70)	7.4	TBAH

Dissolution rates were typically obtained by coating 250 nm of the material on a silicon wafer, baking at 130°C for 60 s, and determining the dissolution rate in LDD-26W with a Luzchem TFA 11. The surface roughness was determined on a Veeco Dimension 5000 AFM with scans performed in tapping mode on a 5 by 5 micrometer square area with 19.5 nm between sampling points. The RMS surface roughness was determined by Veeco analysis software and by the FFT 2D analysis. Both approaches yielded practically identical values with a couple of exceptions when strong global AFM scan distortions existed. The IMR is determined by averaging all measured RMS values for film depths of greater than 50 nm.

All lithographic substrates were HMDS treated 6-inch silicon wafers. The 248-nm exposures employed an organic antireflection coating, Shipley AR3, which was coated to 62 nm on the silicon wafer, followed by a bake of 215°C for 60 seconds. All resists were coated to 250-nm and baked at 140°C for 60 seconds. Following exposure, the resist was baked for 90 seconds at temperatures of either 100 or 130°C. Development was by single puddle with Shipley LDD-26W for 40 seconds. All 248-nm exposures were with a Canon EX-4 248-nm 0.6 NA stepper.

## RESULTS AND DISCUSSION

**FFT 2D and PSD analysis.** The AFM scan is never perfect due to various imperfections of the AFM machine (defined here as baseline), which may affect the shape of the final FFT 2D PSD and its analysis. Accurate approximation of the baseline and its subtraction is a necessary requirement for obtaining a correct PSD and adequate conclusions. Two examples of rough AFM profiles (small and strong baseline distortion) together with the baseline corrected surface profiles and associated PSD spectra are shown in the Figure 1. Here and later for the PSD graphs the vertical axis represents PSD amplitude (in  $\text{nm}^2 * \mu\text{m}$  or normalized), the horizontal axis represents wave number,  $w [1/\mu\text{m}]$  unless it is noted to be different.

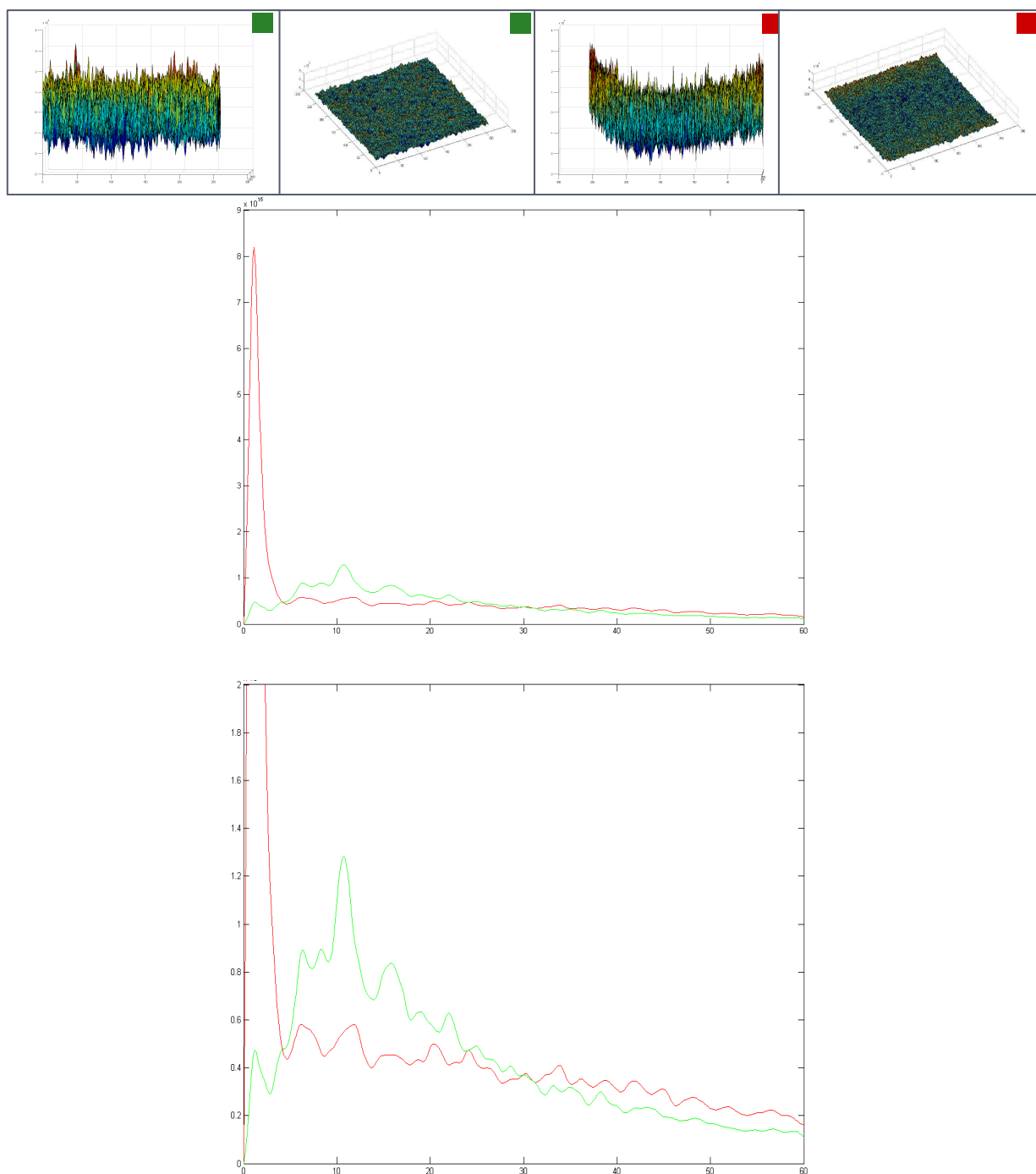


**Figure 1.** Examples of a slightly and significantly distorted AFM scan (side and 3D profiles) together with corresponding PSD spectra are shown (green curves for the slightly distorted case and red curve for the strongly distorted case). The examples demonstrate strong impact in the low frequency range in the case with significant distortion making necessary introduction of an adequate baseline correction routine.

Scan baseline was approximated with a set of polynomial functions and subtracted from the original scan profile. Figure 2 shows the major features of the developed baseline subtraction routine: the original “as scanned” profile, baseline- corrected profile and the side and 3D views of the baseline surface. Top-down

views of original and baseline-corrected surfaces are presented as well. The graphs represent PSD spectra of, correspondingly, the surface “as scanned”, the baseline corrected-surface, and the baseline surface itself. It demonstrates that the baseline subtraction removes mostly the scan bending distortion and practically does not affect the PSD spectrum in the area of interest, which makes it better suited for further analysis. The shape of the baseline surface also could be analyzed for structural content if necessary.

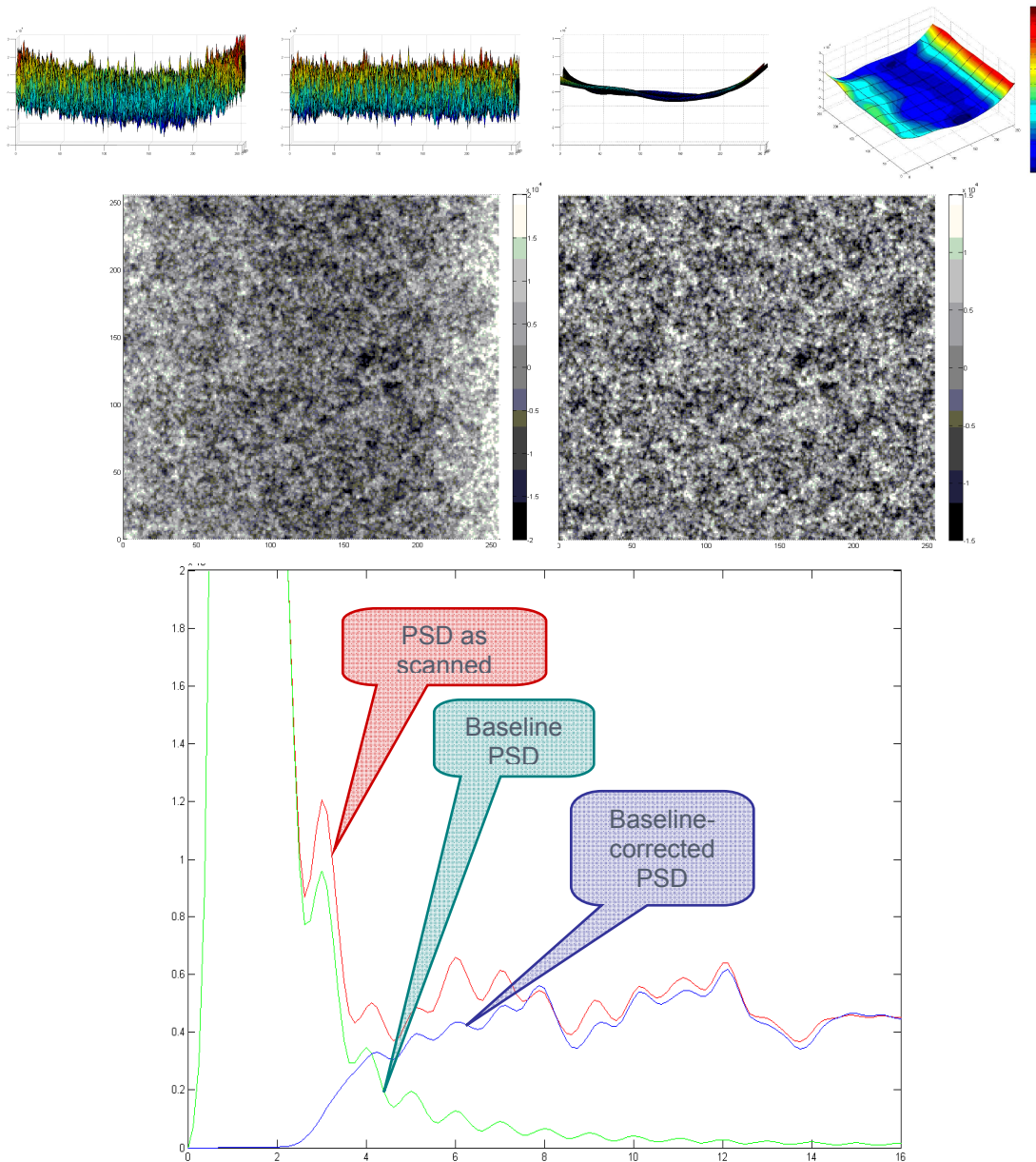


**Figure 2.** Baseline subtraction. The original “as scanned” profile, baseline- corrected profile and side and 3D views of the baseline surface. Top-down views of original and baseline-corrected surface are shown as well. The graphs represent PSD spectra correspondingly of the surface “as scanned”, with baseline correction and the PSD of the baseline surface showing that the baseline subtraction removes mostly the scan bending distortion effects and practically does not affect the PSD spectrum in the area of interest.

As it was mentioned above, the FFT 2D PSD analysis was performed for a large set of Polymer-PAG-Base combinations at various steps of the litho processing sequence (Spin coat-Soft bake- Exposure-PEB), or at various process step parameters, like PEB temperature, for example. Figure 3 presents an example of typical effect associated with film dissolution depth in the developer solvent. Three PSD curves for a particular Polymer-PAG-Base combination at three different dissolution depths, namely, 0 nm (red curve), 58.8 nm (green curve) and 165.4 nm (blue curve) are shown, demonstrating that in general the more film thickness is dissolved the rougher becomes the remaining film surface although the initial “as deposited” film appeared to have practically negligible surface roughness.

Assuming that the residual film surface roughness results from dissolution rate modulation by the film structural non-uniformities, we can conclude that the main contribution to the RMS comes from large  $10^2$  nm sized structures. In other words, structures of this scale seemingly should exist in the bulk of the resist film influencing the resist dissolution rate and shaping the film dissolution front. It also means that to reveal completely this structural modulation the dissolution depth need to be comparable with the largest size of the film structural units. Thermosolutal effects should also be taken into account while discussion the potential source of the dissolution front patterning.

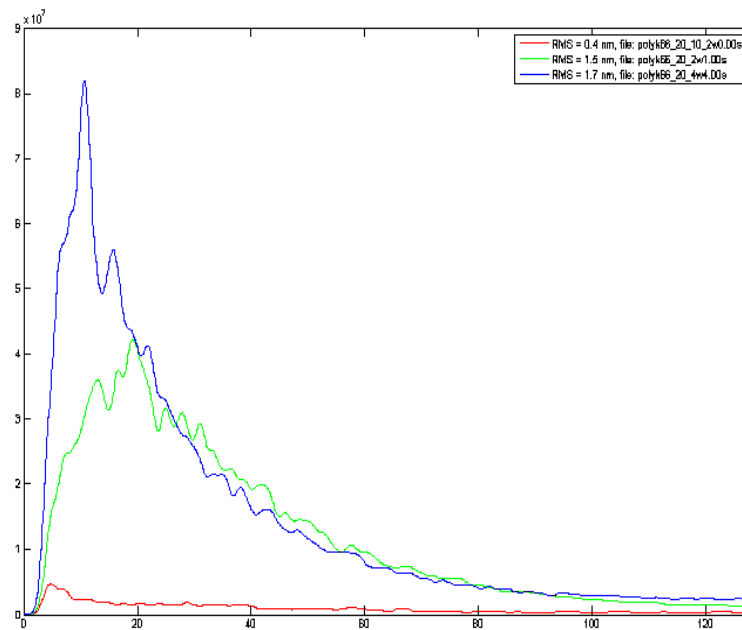


**Figure 3.** FFT 2D PSD spectra for three film dissolution depths, 0 nm (red curve), 58.8 nm (green curve), and 165.3 nm (blue curve), demonstrating that the main contribution to the RMS comes from large  $10^2$  nm sized structures. Structures of this scale seemingly exist in the bulk of the resist film modulating the resist dissolution rate and shaping the film dissolution front. It also means that the deeper the dissolution front propagates the more pronounced become the details associated with the internal resist film structures (intrinsic or induced by the film processing)

Figure 4a offers an example of a set of depth profiling FFT 2D PSD spectra (22 depth levels) for a particular combination of polymer/PAG/Base at a particular set of resist processing conditions with both spectral amplitudes and spectral features varying over a wide interval, making their analysis very complicated. Some improvement comes with normalization: being normalized to the maximal amplitude (Figure 4b) the spectra clearly show that depending on depth, different wave numbers prevail in the PSD spectra.

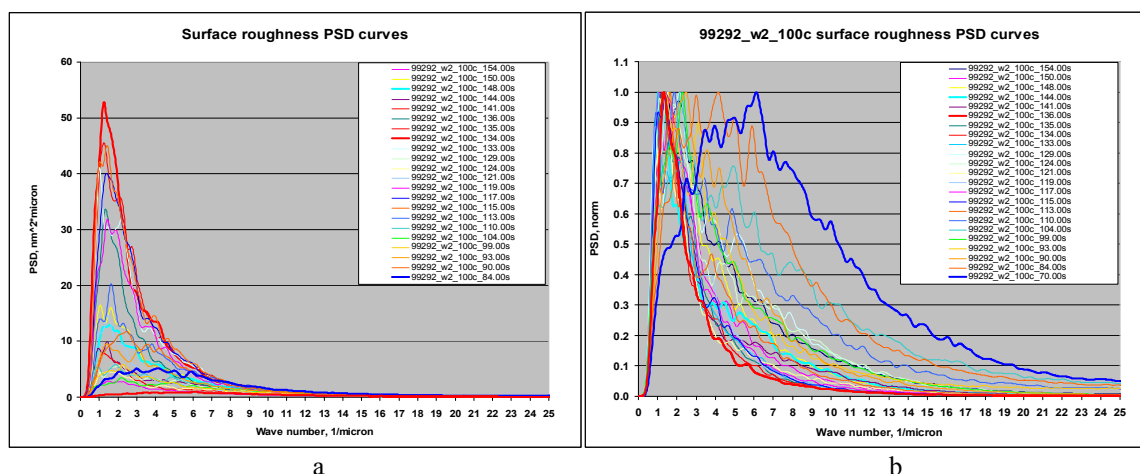
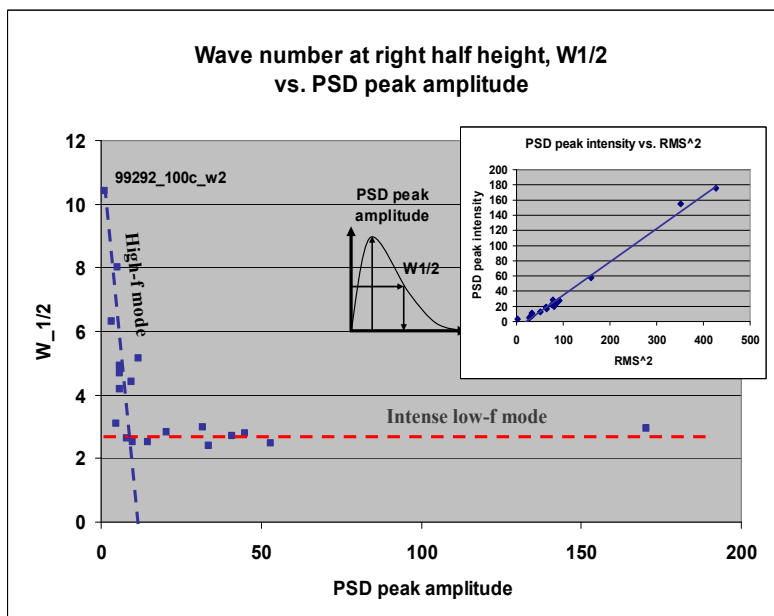


**Figure 4.** FFT 2D Power Spectral Density (PSD) curves (a-actual, b- normalized)

A more advanced analysis of PSD curves shape variation was performed by plotting the position of the PSD right wing, at half height,  $W_{1/2}$  vs. PSD peak amplitude (see the inset in Figure 5). This analysis clearly revealed by-modal nature of the PSD spectra, which appeared in the prevailing number of cases tested.

For most of the resist components/conditions combinations the set of  $W_{1/2}$  values was found to be divided into two sub-sets, with one following a low frequency trend (or blue dotted low-f mode in Figure 5), and the other part following a high frequency trend (red-dotted high-f mode in Figure 5).

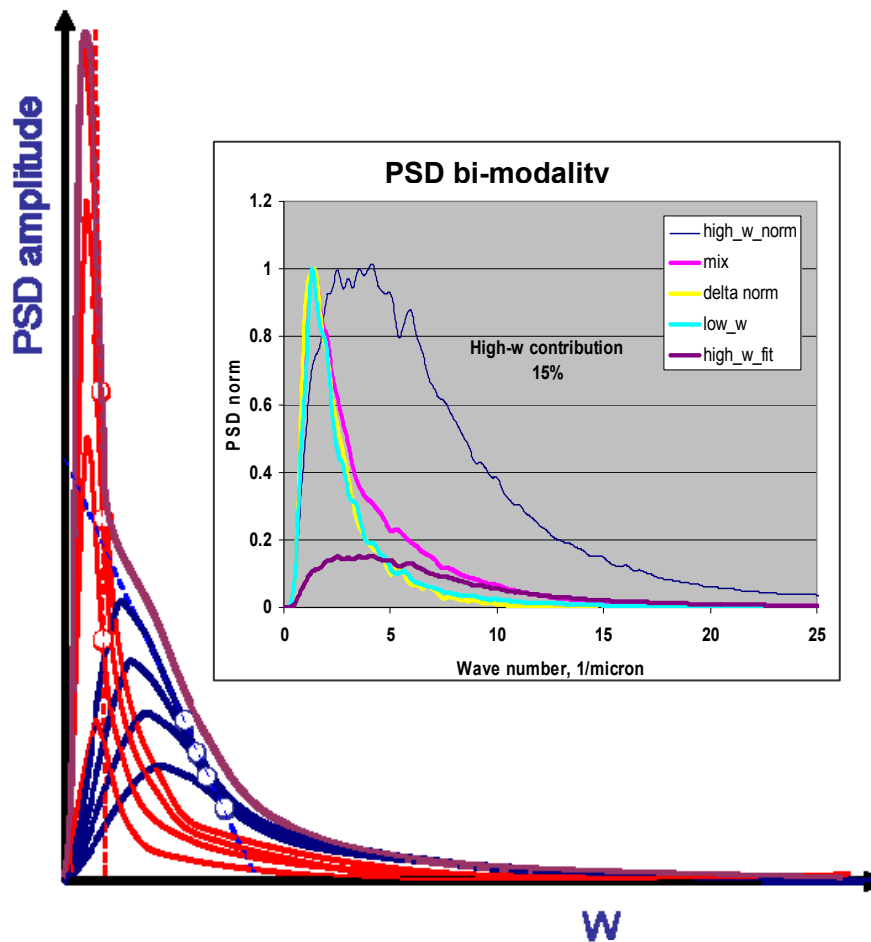
PSD peak amplitude was found to be in a good linear correlation with the  $RMS^2$  value.



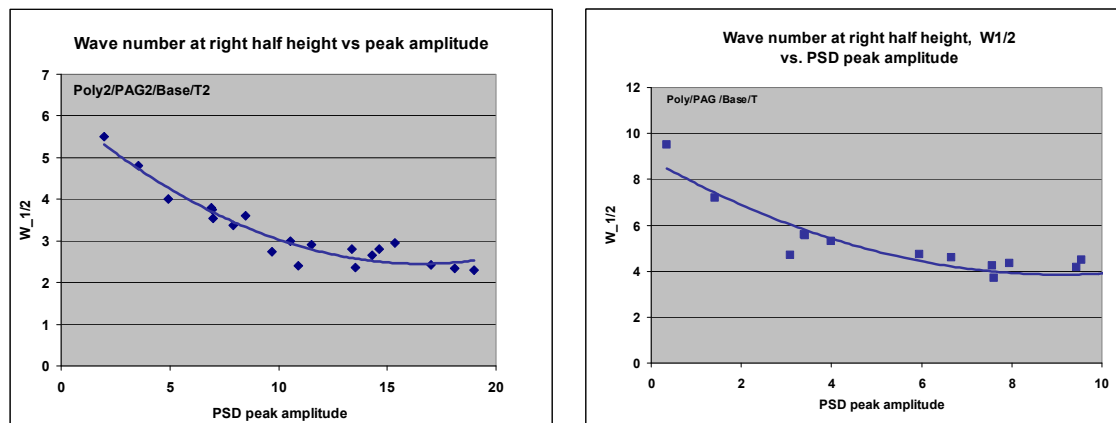
**Figure 5.** Analysis of PSD spectra shape variation ( $W_{1/2}$  vs.  $PSD_{max}$ ) demonstrating roughness bi-modality. The insert demonstrates a linear correlation between the  $RMS^2$  and  $RSD_{max}$ , well repeatable for all combinations tested.

Figure 6 presents a set of schematic PSD curves illustrating the essence of bi-modality. Two phenomena, one characterized by a wider PSD spectrum extended to higher frequencies, and the other with a tighter spectrum localized mainly in the low frequency region, are jointly contributing to the overall surface roughness. At some specific set of depth/conditions the high frequency phenomenon (smaller size of roughness asperities) dominates and the overall PSD looks like the solid blue curve in graph 4b. At the other set of conditions the low frequency phenomenon (smaller size of roughness asperities) dominates, and the overall PSD spectrum looks like the solid red curve in graph 4b. And, certainly, a variety of mixed cases occurred for intermediate conditions. An example of a mixed case is presented in the inset of Figure 6. It is shown that a mixed case PSD spectrum (magenta curve) could be represented as a linear combination of the low frequency (turquoise and yellow curves) and high frequency (blue curve) PSD distributions.

As shown in Figure 6, until the high frequency phenomenon dominates the  $w_{1/2}$  values follow the blue dotted line, and they turn to follow the red one after the low frequency phenomenon becomes a dominant one. The clear bi-modality case was found to be a very frequent one. However, in some cases such well-separated bi-modality appeared less clear or did not appear at all (examples shown in Figure 7).



**Figure 6.** To the explanation of the FFT 2D PSD spectra bi-modality. Insert: an example of a mixed case with a comparable linear contributions of both lower and higher frequency modes.



**Figure 7.** Examples of cases with not well-separated bi-modality

Numerous variations in PSD spectra associated with resist composition, process steps, and process conditions were analyzed and the respective conclusions drawn, and we are planning to publish these data in a separate paper. In this publication we discuss the approach itself and one major finding, which should be considered as very important for the understanding the basics of the resist performance.

## SUMMARY

Based on the PSD spectra shape analysis a generally fundamental conclusion critically important for understanding and fixing the LER/LWR issues was reached. Most of the sets of the PSD spectra exhibited a pronounced bi-modal structure, indicating that there are at least two clearly noticeable independent roughness-controlling mechanisms:

- One of a generally smaller amplitude and higher frequency (smaller size of roughness features, < 200 nm), and
- Another one of higher amplitude and lower frequency (larger size of roughness features, < 1000 nm).

In such a complex case, a statistical analysis based on a single phenomenon, such as shot noise associated with CAR processing, should be considered as insufficient to account for the variations in surface roughness PSD spectra.

Another important conclusion is based on the analysis of the properties of the low frequency phenomenon, which was found to be the major roughness contributor. Indeed, that large size scale of the roughness features (about 1000 nm) could not be associated with the acid diffusion and should be attributed to a different, much larger scale phenomenon.

The last point to touch in this discussion is the following: what helped us observe these informative fine structural variations in the PSD spectra, and why they were not detected by other researchers in previous works? The shapes of our PSD spectra were found to agree well with the data from numerous other previously published works once our data were plotted on a log-log scale. Not too much structural information could be extracted from the PSD curves in this case. Therefore, we strongly believe that in contrast to log-log plot analysis, which wipes out the fine structural information, the linear scale approach that we have employed is much more productive, allowing getting a realistic insight in the origin of resist roughness.

## ACKNOWLEDGMENTS

We are very thankful to Keith Standiford for his discussion remarks as well as for assistance in editing this paper. We would like to acknowledge the MEL lithography team from Lincoln Laboratory for performing the lithography. We would like to thank Michael Sheehan and Matt Romberger of DuPont Electronic Polymers for providing the polymers used in this study. The Lincoln Laboratory portion of this work was sponsored by the Defense Advanced Research Projects Agency under Air Force Contract FA8721-05-C-0002. Opinions, interpretations, conclusions, and recommendations are those of the author, and do not necessarily represent the view of the United States Government.

## References

- [1] Pawloski A, Acheta A, Lalovic I, La Fontaine B, and Levinson H., "Characterization of line-edge roughness in photoresist using an image fading technique", Proc. SPIE 5376, 414-425 (2004).
- [2] Kruit, P., Steenbrink, S., Jager, R., and Wieland, M., J. Vac. Sci. Technol. B 22, 2948 (2004).
- [3] Kruit, P., Steenbrink, J. Vac. Sci. Technol. B 23, 3033 (2005).
- [4] G. M. Gallatin, Proc. SPIE, 5754, 38 (2004).
- [5] Gallatin, Gregg M., Naulleau, Patrick, Niakoula, Dimitra, Brainard, Robert, Hassanein, Elsayed, Matyi, Richard, Thackeray, Jim, Spear, Kathleen, Dean, Kim, " Resolution, LER and sensitivity limitations of photoresists," Proc. SPIE, 6921, 69211E-69211E-11 (2008).
- [6] *Yehiel Gotkis*. Interfacial Dynamic Mesoscopic Structuring As a Highly Probable Origin of the LER Mysterious Fundamental 5nm-Limit, at 2007 Lithography Workshop, Puerto Rico, 2007
- [7] Fedynyshyn, T. H., Sinta, R. F., Astolfi, D. K., Cabral, A., Roberts, J. M., and Meagley, R., "Deconstructing the resist to probe innate material roughness," Proc. SPIE 6153, 615315 (2006).
- [8] Roberts, J. M., Meagley, R., Fedynyshyn, T. H., Sinta, R. F., Astolfi, D. K., Goodman, R. B., and Cabral, A., "Contributions to innate material roughness in resist," Proc. SPIE 6153, 61533U (2006).
- [9] Fedynyshyn, T. H., Sinta, R. F., Astolfi, D. K., Cabral, A., Roberts, J. M., and Meagley, R., "Resist deconstructon as a probe for innate material roughness," J. Microlith., Microfab., Microsyst. 5, 043010 (2006).
- [10] Fedynyshyn, T. H., Pottebaum, I., Astolfi, D. K., Cabral, A., Roberts, J. M., and Meagley, R., "Contribution of photoacid generator to material roughness," J. Vac. Sci. Technol. B 24, 3031 (2006).
- [11] Woodward, J. T., Fedynyshyn, T. H., Astolfi, D. K., Cann, S. G., Roberts, J. M., and Leeson, M. J., "Component segregation in model chemically amplified resists," Proc. SPIE 6519, 651915 (2007).